Slab Rollback Orogeny model: A test-of-concept

Luca Dal Zilio[1,2*], **Edi Kissling**[1], **Taras Gerya**[1], **Ylona van Dinther**[1,3]

[1] Department of Earth Sciences, ETH Zürich, Sonneggstrasse 5, 8092 Zürich, Switzerland
[2] Seismological Laboratory, California Institute of Technology, 1200 E California Blvd, Pasadena, USA
[3] Department of Earth Sciences, Utrecht University, Princetonlaan 8A/4, Utrecht, Netherlands

Key Points:

- 2-D seismo-thermo-mechanical modeling is performed to investigate the driving forces during the post-collisional stages
- Post-breakoff residual slab proves sufficient to sustain slab rollback and retreat of the entire orogen
- The proposed scenario is consistent with the post-collisional seismotectonic evolution of the central European Alps

* Corresponding author: Luca Dal Zilio, dalzilio@caltech.edu

This article has been accepted for publication and undergone full peer review but has not been through the copyediting, typesetting, pagination and proofreading process which may lead to differences between this version and the Version of Record. Please cite this article as doi: 10.1029/2020GL089917

Abstract

Buoyancy forces associated with subducting lithosphere control the dynamics of convergent margins. In the post-collisional stage these forces are significantly reduced, yet mountain building and seismicity are ongoing, albeit at lower rates. We leverage advances of a newly developed seismo-thermo-mechanical modeling approach to simulate tectonic and seismicity processes in a self-driven subduction and continental collision setting. We demonstrate that the rearrangement of forces due to slab breakoff, in the post-collisional stage, causes bending and rollback of the residual slab, suction forces and mantle traction at the base of the upper plate, while stress coupling transfers to the shallow crust. Our results provide an explanation for the post-collisional evolution of the Central Alps, where the so-called *Slab Rollback Orogeny* models explains the slow yet persistent upper plate advance, the height of the mountain range, and a seismicity pattern consistent with the different tectonic regimes throughout the orogen.

Plain Language Summary

A long-standing debate in tectonophysics evolves around whether vertical or horizontal forces are the primary drivers of mountain building processes. Here we explore this problem using 2D numerical models in a generic subduction and continental collision setting. Our results show how the post-collisional evolution of the orogen is controlled by a slow, but persistent, sinking and bending of the post-breakoff residual slab. The resulting seismicity pattern shows a broad pattern of different style of faulting, which are consistent with the local tectonic regimes. We find good correlations between our numerical results and the previously conflicting tectonic observations in the Central Alps and the adjacent foreland basin. Our results thus support the hypothesis that the post-breakoff remaining slab exerts a first-order control on the motions and deformations of collisional orogens.

1 Introduction

The process of continent-continent collision in shaping mountain ranges and adjacent foreland basins have intrigued geoscientists for decades (e.g., Beaumont et al., 1996; Forsyth and Uyeda, 1975; Malinverno and Ryan, 1986; Uyeda and Kanamori, 1979; Whipple and Meade, 2006). According to the most commonly used conceptual models, the evolution of mountain belts is largely driven by the horizontal convergence between the two colliding plates (e.g., Handy et al., 2010; Schmid et al., 1996). This view is based on the perception in which a rigid indenter — frequently exemplified by a bulldozer — in combination with kinematic convergence leads to mountain building processes (e.g., Willett, 2010, for a review). These mechanisms have been invoked to explain the accretion of crustal units from both the upper and lower plates, the building of topography, and the surface denudation of the accreted material (e.g., Beaumont et al., 1996; Whipple, 2009).

Similar kinematic assumptions can potentially be applied to the Central Alps (Fig. 1) to investigate crustal accretion and surface erosional processes on both the

orogen and the adjacent foreland basins. However, models based on these assumptions are problematic in several aspects as they underestimate the depth of the crust-mantle boundary (i.e., Moho) beneath the core of the orogen of >50%, and overestimates the mean topography elevation when principles of isostatic equilibrium are applied (Kissling, 1993). Further, under these assumptions the strong negative Bouguer anomalies measured in the Central Alps cannot be explained (Lyon-Caen and Molnar, 1989). The crustal roots in the Central Alps have been seismically determined to be ~60-km thick (Fig. 1c), and thus far out of conventional isostatic equilibrium with a mean surface topography of only ~2 km (Kissling, 1993). This evidence leads to the notion that the Alpine roots are overcompensated by many kilometers. How to reconcile this with models of orogenic evolution remains unclear.

A more recent, alternative explanation suggests that sinking and bending of >180-km-long European lithospheric mantle, in addition to topographic loads, are required to maintain the mountain range close to force equilibrium and to sustain the Alpine topography (Schlunegger and Kissling, 2015). This revised view on the Central Alpine Orogeny, which we refer to as *Slab Rollback Orogeny* (SRO) model (Kissling and Schlunegger, 2018), suggests that the post-collisional evolution of Central Alps evolved in response to a slab rollback process, in which the buoyancy forces of a retreating subduction are driven by the well-known concepts of slab sinking and retreat (Brun and Faccenna, 2008; Malinverno and Ryan, 1986; Royden, 1993), and force balance (Forsyth and Uyeda, 1975). According to the SRO model, slab sinking and bending-related suction forces have been sufficiently strong to drag the overriding Adriatic microplate throughout the long-term subduction and collision, and even during post-collisional convergence (i.e., after slab detachment). Such a rollback mechanism provides a dynamically consistent mechanism to explain the construction of thick sedimentary successions in the Molasse basin where the extra slab load has maintained the Alpine surface at moderate elevations (Schlunegger and Kissling, 2015). Finally, the SRO model provides a viable mechanism to explain the seismicity pattern beneath the Molasse foreland basin, where middle to lower crustal earthquakes (20–30 km deep) are predominantly characterized by bending-related normal-faulting events (Singer et al., 2014) (Fig. 1c). This leads to the hypothesis that sinking and bending of the remaining slab have been at work beneath the Central Alps, at least in the last ~20 My.

Thus far, numerical models of subduction have widely been used to study, e.g., mantle-lithosphere interactions (e.g., Billen, 2008; Capitanio et al., 2010; Dal Zilio et al., 2018a), continental collision processes (e.g., Faccenda et al., 2009; Magni et al., 2014; Pusok et al., 2018), surface denudation (e.g., Erdős et al., 2019; Willett, 1999), as well as slab breakoff (e.g., Davies and von Blanckenburg, 1995; Duretz et al., 2011; Magni et al., 2013; van Hunen and Allen, 2011). However, less work has been done in studying the post-collisional dynamics. In particular, the open question is whether buoyancy forces and mantle-lithosphere interaction are capable of sustaining the retreat process of a collisional orogen, even after slab breakoff. In this study, we leverage

advances of a newly-developed, 2-D seismo-thermo-mechanical (STM) model to simulate both the long-term tectonic and the short-term seismicity of a generic convergent margin, from subduction to collisional orogeny. Our intent here is to investigate the interplay and balance between driving and resisting forces as well as plate motions and crustal deformations. This allows probing how driving and resistive forces control the dynamics, tectonics, and seismicity of a post-collisional margin. Lastly, we discuss possible applications of our model to the Central Alps collision system.

2 Seismo-Thermo-Mechanical (STM) modeling

We perform simulations using the 2-D, continuum-based, finite difference code STM (van Dinther et al., 2013). This modeling framework utilizes a fully staggered Eulerian grid and freely advecting Lagrangian markers storing the rock properties (Gerya and Yuen, 2003). Conservation of mass, momentum, and heat are implicitly solved for an incompressible medium on the Eulerian grid, whereas physical properties are interpolated to the markers for advection (Gerya and Yuen, 2007). The mechanical equations include inertia and gravity and the thermal equation includes the effect of radioactive and shear heating, as well as adiabatic heat production/consumption (see Supplementary Information). Solid-solid phase transformations and density crossover (e.g., eclogitization) are employed via parameterization of phase boundaries using polynomials to interpolate the reaction boundary (Faccenda and Dal Zilio, 2017).

We employ non-Newtonian visco-elasto-plastic rheologies (Gerya and Yuen, 2007). The effective viscosity is calculated from experimentally constrained dislocation creep flow laws (Table S1). The brittle-plastic behaviour is taken into account assuming a non-associative Drucker–Prager yield criterion. Frictional instabilities and healing are introduced by a strongly rate-dependent friction formulation in which the effective friction depends on the slip velocity, which is calculated from the visco-plastic strain rate and effective fault width. When the time step is 1 yr, our formulation is reduced to a virtually quasi-dynamic one; however, because of a relatively large smallest time step, our models produce unrealistically long seismic events. Rupture events hence represent the occurrence of rapid slip during which permanent deformation and stress drop occur along a localized plastic shear zone. Nonetheless other observables, such as slip, surface displacements, rupture widths, and magnitude sizes, agree with natural observations (e.g., Dal Zilio et al., 2018b; van Dinther et al., 2013). The key strength of this invariant formulation allows for spontaneous localization and faulting at any orientation. This means that, instead of being a priori defined, the spontaneous development of faults is governed by local stress and strength states.

The initial model domain consists of two continental plates separated by an oceanic basin (Fig. 2a and S1). The dimensions of the computational domain is 3000 x 1200 km^2 (1921 x 347 nodes), and all the boundary conditions are free slip. We use a variable grid spacing, which enables to reach a grid resolution of 400 m in the central part of the domain where the continental collision takes place. Subduction

initiation is imposed during the early phases of the numerical experiment assuming a 25° dipping weak zone (low plastic strength) on the right ocean–continent transition (Fig. 2a). During this period, the oceanic subduction is kinematically prescribed with a fixed convergence rate of 10 cm/yr until 200 km of the oceanic slab is subducted into the mantle. After this model initialization step, the convergence rate is removed and the model is self-driven by internal, buoyancy forces. In this way, the long-term evolution is self-driven and not steady state, as it depends on the slab pull, dissipative forces, and crustal buoyancy. The visco-elasto-plastic thermo-mechanical parameters of each lithology are based on a list of laboratory experiments (Table S1). An extended description of the numerical methodology, model setup, and modeling procedure is given in the Supporting Information.

3 Results

We present results from the reference model displaying the long-term subduction, collision and oceanic slab breakoff. We examine how sinking and flexural bending of the remaining slab controls the post-collisional tectonic evolution of the orogen. We then simulate the short-term seismicity pattern and compare it with that of the Central Alps. This comparison allows us to better understand how long-term dynamics relates to the present-day seismicity and crustal tectonics in the Central Alps. Lastly, we explore the sensitivity of our results by varying the age of the oceanic plate (Table S2), which in turn affects its temperature, density contrast (negative buoyancy), and strength (see Supplementary Information).

3.1 Stage 1: Subduction, collision, and slab breakoff

After an initial stage of kinematically imposed subduction initiation, oceanic lithosphere sinks spontaneously at the ocean-upper plate continental margin. Self-sustaining retreating subduction causes the migration of the trench and exerts a suction force to the upper continental plate, while the subduction-induced mantle flow maintains the upper plate highly coupled with the retreating slab (Fig. 2b,c). Toward the onset of continental collision and indentation, sediments are accreted in the orogenic prism, while the upper plate acts as a buttress. The buoyancy of the continental crust slows down subduction and, hence, the convergence, though a non-negligible part of continental lithosphere is still being subducted. The collisional zone thus achieves an asymmetric architecture with a doubly-vergent thrusting pattern. Slab necking occurs at a relatively shallow depth of approximately 240 km during the stage of slab steepening (Fig. S2). Breakoff occurs at the ocean-continent transition a few million years after the collision stage initiated. Slab breakoff and subsequent rebound produces a sharp topographic signal, which results in an uplift rate of $\sim$0.5 mm/yr due to a rebound of $\sim$1 km in $\sim$2 My. Such uplift is modulated by the rate of removal of overburden by erosional processes. A simulation example is shown in Supplementary Movie S1.

3.2 Stage 2: Post-collisional slab rollback evolution of the orogen

Our numerical experiments indicate that slab detachment is responsible for a stress redistribution within the subducting lithosphere and throughout the orogen. Partial loss of slab pull is followed by a transient (<2-My-long) elastic unbending of the remaining slab and an isostatic rebound of the orogenic wedge (Fig. S3–5 and Movie S1). After this transient period, our numerical simulations show that the negative buoyancy — offered by the remaining slab — remains the dominant driving force in the collisional system (Fig. 3a), although at lower sinking rates. Slow yet persistent sinking and bending of the remaining slab results in the migration of the whole orogen towards the foreland basin (Fig. S3–5). The ongoing rollback is accompanied by crustal shortening and stacking, which cause shortening on the frontal part of the orogen and in the foreland basin. At deeper crustal levels, buoyant crustal materials is delaminated, while the lower crust continues to subduct at a low, but detectable, sinking rate (Fig. 3a and S3). In addition, heat diffusion decreases the flexural strength of the lower plate. This thermo-mechanical process increases the curvature of the lower plate in the asthenosphere, and thus closer to a thermoelastic relaxation of a continental plate to applied loads.

3.3 Stage 3: Regional stresses and seismicity distribution

Results from the seismic cycle simulations show a wide domain subjected to brittle faulting. Seismogenic deformation in the orogenic wedge is largely driven by extensional stresses resulting from the development of retreating subduction (Fig. 3b and S3–5). Because of the yielding of the upper plate, the orogenic wedge partially overthrusts the retro-foreland domain. High compressional stresses are transferred on the upper plate, thus causing a development of a sequence of seismogenic thrusts at the front and beneath the retro-foreland basin (Fig. 3b). Deep earthquakes beneath the foreland basin extend into the lower crust and their distribution correlates well with the flexural bending of the gently to steeply dipping downgoing plate. Flexural bending thus transfers stresses into the lithosphere beneath the foreland basin. Consequently, tectonic stress transfer in the lower and upper crust beneath the foreland results in compressional stresses in the shallower domains and an extensional domain at deeper crustal levels (Fig. S6). The laterally variable rheological contrasts between the deeper crustal roots and the brittle shallow crust explain the depth dependency of the seismicity pattern. Lastly, these results illustrate how the long-term tectonic evolution and crustal properties affect the architecture of the orogen and thereby their short-term spatial distribution of seismicity.

4 Discussion

4.1 Slab Rollback Orogeny Model: Driving and Resistive Forces

The dynamic behaviour of subduction systems is governed by the force balance between stresses induced by the buoyancy of the slab and by the viscous flow of the surrounding mantle (Davies, 1977; McKenzie, 1969; Stevenson and Turner, 1977; Turcotte and Oxburgh, 1967). Our results show that such dynamic behaviour holds even during the syn- post-collisional phases, although at very reduces rates. Despite partial loss of the negative buoyancy due to slab breakoff, the post-collisional sinking and flexural bending of the remaining slab is still capable of sustaining slab retreat and suction of the upper plate (Fig. 3a).

In our numerical experiments, the main driving force responsible for the motion of tectonic plates is the slab sinking force (i.e., negative buoyancy), which is defined as:

$$F_s = \int \int_A \bar{\rho}_m(z) - \bar{\rho}_s(z)\, g \;\, dx\, dz, \tag{1}$$

where $\bar{\rho}_m$ and $\bar{\rho}_s$ stand for the mean mantle and slab density at a given depth (z), respectively, whereas g is the acceleration of gravity and A the 2-D area of the slab. After detachment, the reduced slab area yields to a F_s of $\sim 8{-}9{\cdot}10^{12}$ N/m. In response to slab sinking, poloidal mantle flow is induced in front of the slab tip, which in turn generates basal shear stresses beneath the overriding plate (Fig. 4a,b). Notably, our models show that shear stresses localizes at a characteristic length ($L_c \approx 180$ km; Fig. 4d), which corresponds to the effective length of the remaining slab. We then compute the magnitude and time-evolution of mantle flow traction force by integrating shear stresses at the base of the overriding plate (Fig. 4e):

$$F_t = \int_{L_{up}} \sigma_{xy}\, dx, \tag{2}$$

where L_{up} is the length of the upper plate, whereas shear stresses are proportional to the upper mantle viscosity and the vertical gradient of the horizontal velocity. After slab detachment, basal traction beneath the upper plate initially grows over time (Fig. 4e); however, when the slab becomes (sub-)vertical and the bending moment is released, the sinking rate slows down. As a result, the response of mantle flow and the basal traction beneath the upper plate diminish.

Our results indicate that, when the underlying continental crust is dragged into the mantle to depths of ~110–120 km, large buoyancy forces are generated and slab sinking slows down. These deep crustal domains are then warmed up, delaminated, and extruded (Movie S1). According to our results, the forward migration of the mountain range towards the foreland basin, coeval with crustal deformation — ductile at depth and brittle at shallower levels — is governed by a combined effect of slab sinking and bending, and buoyancy forces of the crustal root. More importantly, these processes create a positive feedback as delaminated material from the lower plate increases the relative importance of the vertical slab load, thus promoting further down warping

of the plate. Also, this mechanism localizes extensional stresses both at the Moho and within the lower crust (Fig. 4c and S6), with the consequence of intra-crustal seismicity at both shallow and deep crustal levels (Fig. 3b).

The mantle-lithosphere interaction observed in our models emerges naturally and explains why the upper and lower continental plates are mechanically coupled even in the absence of any pre-imposed convergence rate (Fig. 4a,b and S3). Extensional and compressive stresses coexist across the orogen and at different depth levels (Fig. 4f). Within the lithospheric mantle, horizontal stresses propagate from the lower plate to the upper plate. The lower plate is subjected to an in-plane force and a bending moment, which depend on the magnitude of the slab sinking force. The resulting lithospheric flexure leads to extensional stresses within the bending region, while large suction forces propagate across the plate interface triggering compressional stress within the lower plate (Fig. 4c). At shallower crustal levels, horizontal stresses are generally lower. Notably, the underlying dynamics results in a compression-extension-compression regime. Intra-orogenic extension is ascribed to a combination of buoyancy-driven extrusion of the crustal roots and gravitational potential energy governed by the topographic and crustal thickness variation between the mountain range and hinterland. As a result, compressional stresses are transmitted on both the pro-foreland and retro-foreland basins.

Note that the SRO model develops for certain age of the oceanic plate (Table S2). The age of the downgoing slab has a first-order effect on the temperature structure, density contrast (i.e., negative buoyancy), and stiffness of the lithosphere. By varying the plate's age, we find that the older the plate, the deeper the slab breakoff (Fig. S7–S14). In particular, the age-dependent sinking of the remaining slab depends on its post-breakoff length, as it modulates the sinking force and, in turn, the characteristic length (L_c) and magnitude of mantle flow traction at the base of the upper plate. On the one hand, when slab breakoff is shallow (Fig. S8–S10), the post-collisional dynamics are negligible and the seismicity is entirely restricted to a few events within the orogen (Fig. S15a). On the other hand, when the SRO model emerges (Fig. 3 and S15b), the seismicity pattern predicts a distribution of earthquakes similar to that observed in the Central Alps (Fig. 1c). In our models, the post-collisional retreat of the remaining slab and buoyancy forces control the dynamic coupling and tectonic stress transfer between the upper and lower plates and within the orogen. Such a stress transfer leads to seismic events with a compressional component beneath the foreland basin and in the upper plate, and with an extensional component in the lower crust and in the core of the orogen.

4.2 Slab Rollback Orogeny Model for the tectonic evolution of the Central Alps

A first-order comparison between our results and the Central Alps (Fig. 1) shows some interesting similarities at the scale of the orogen. The dynamic evolution

of our model is consistent with palaeomagnetic evidence that the lower (European) continental plate has remained nearly stationary since the Late Cretaceous (Dewey et al., 1989), while the upper continental plate was decoupled from Africa and converging against Europe (Platt et al., 1989). This means that the subduction of the Alpine Tethys occurred through a rollback process, and it continued through the syn- and post-collisional phases (Froitzheim et al., 1997). Teleseismic tomography cross-sections have shown that, along the NW–SE transect across the Central Alps (Fig. 1b), the slab dips with only ∼60° (Kästle et al., 2019; Lippitsch et al., 2003), suggesting that the remaining slab beneath the Central Alps might still be subjected to a bending moment and an axial force. Seismic anisotropy studies suggest that imbricate stack of lower crustal material — delaminated from the European crust — is consistent with a rollback process (Fry et al., 2010). Notably, our reference model reproduces an isostatic balance between the ∼60-km-thick buoyant crustal roots and the negative buoyancy provided by the remaining slab, which modulates the sinking rate and the relatively low orogen' topography. The orogen, like for the Central Alps, sits mostly on the lower continental plate, with a topography that does not exceed 5 km in height. The post-collisional convergence rate is relatively small (2-3 mm/yr; Fig. 4c), and in agreement with GPS measurements (Calais et al., 2002). Finally, from 10 to 20 My after slab breakoff, crustal shortening propagates towards the foreland basin, similarly to the shallow crustal shortening observed in the Jura thrust belt over the last 10 Ma (e.g., Burkhard, 1990).

In terms of the detailed architecture of the orogen, the presented modeling results are largely simplified compared to the much more complicated Alpine system. Our model does not include three-dimensional effects of a collisional margin (e.g., Magni et al., 2017; Pusok et al., 2018), including the interaction between subducting slabs (e.g., Király et al., 2016), and magmatism (e.g., Menant et al., 2016). Also, even excluding along-strike variations of the Alpine arc, details of each individual tectonic structure cannot be expected to be reproduced in a self-driven, generic model such as the ones of this study. On the other hand, the advantage of this model setup is the possibility of simulating a generic convergent margin, and analyzing the driving forces and seismic behavior acting on the system.

5 Conclusions

This work focuses on the post-collisional evolution of orogens. Our results show the terminal stage of collision and slab breakoff demonstrating that, although driving forces are significantly reduced, the negative buoyancy offered by the remaining slab is sufficient to control the evolution of post-collisional orogens. Sinking and bending of the remaining slab cause suction forces towards the plate boundary and mantle tractions force at the base of the upper plate. The thermal age of the detached oceanic plate is crucial for the occurrence of the SRO process, as it controls the mantle flow through density contrast (negative buoyancy) and depth of slab breakoff, setting the

characteristic distance under which basal shear stresses localize. Competition between the negative buoyancy of the remaining slab and thick buoyant crustal roots modulates slab sinking, thus maintaining the orogens' topography relatively low.

This so-called *Slab Rollback Orogeny* model offers an explanation for the ensemble of observations extracted from the Central Alps (Kissling and Schlunegger, 2018), including (1) the stacking of nappes (Fry et al., 2010), (2) the force balance with the thick and buoyant crustal root, (3) the post-collisional evolution of the Molasse foreland basin (Schlunegger and Kissling, 2015), and (4) the current seismicity pattern in the Central Alps (Singer et al., 2014). Notably, slab retreat and upper mantle confined dynamics are features commonly found in other post-collisional convergent margins, including the Apennines (e.g., Carminati et al., 2003; D'Acquisto et al., 2020) and in most of the circum-Mediterranean arc (Brun and Faccenna, 2008; Faccenna et al., 2004; Jolivet et al., 2013; Royden, 1993). In light of these results, while the evolution of the Himalayas serves as a much better example where mountain building processes and collision are ongoing, the understanding of the recent geologic history of the Central Alps requires an alternative view.

Acknowledgments

This study was funded by the Swiss National Science Foundation (SNSF) SwissAlpArray SINERGIA (`2-77090-14`), the Early Postdoc.Mobility fellowship (`P2EZP2_184307`), and the Drinkward Fellowship at Caltech. Numerical simulations were performed on ETH cluster Euler. This work has benefited from several discussions with F. Capitanio. We thank M. Gurnis, W. Spakman, M. Faccenda, B. Kaus, G. Pozzi, K. Ueda, and A. Ceccato for constructive comments. We thank the editor and two anonymous reviewers for their valuable comments and suggestions for improving the manuscript. Figures were made using perceptually uniform colormaps (Crameri, 2018). Data related to this study can be downloaded from the following link: http://dx.doi.org/10.22002/D1.1376

References

Beaumont, C., Ellis, S., Hamilton, J., and Fullsack, P. (1996). Mechanical model for subduction-collision tectonics of alpine-type compressional orogens. *Geology*, 24(8):675–678.

Billen, M. I. (2008). Modeling the dynamics of subducting slabs. *Annu. Rev. Earth Planet. Sci.*, 36:325–356.

Brun, J.-P. and Faccenna, C. (2008). Exhumation of high-pressure rocks driven by slab rollback. *Earth and Planetary Science Letters*, 272(1-2):1–7.

Burkhard, M. (1990). Aspects of the large-scale miocene deformation in the most external part of the swiss alps (sub-alpine molasse to jura fold belt). *Eclogae Geologicae Helvetiae*, 83(3):559–583.

Calais, E., Nocquet, J.-M., Jouanne, F., and Tardy, M. (2002). Current strain regime in the western alps from continuous global positioning system measurements,

1996–2001. *Geology*, 30(7):651–654.

Capitanio, F., Stegman, D., Moresi, L.-N., and Sharples, W. (2010). Upper plate controls on deep subduction, trench migrations and deformations at convergent margins. *Tectonophysics*, 483(1):80–92.

Carminati, E., Doglioni, C., and Scrocca, D. (2003). Apennines subduction-related subsidence of Venice (Italy). *Geophysical Research Letters*, 30(13).

Crameri, F. (2018). Scientific colour-maps.

D'Acquisto, M., Dal Zilio, L., Molinari, I., Kissling, E., Gerya, T., and van Dinther, Y. (2020). Tectonics and seismicity in the northern apennines driven by slab retreat and lithospheric delamination. *Tectonophysics*, page 228481.

Dal Zilio, L., Faccenda, M., and Capitanio, F. (2018a). The role of deep subduction in supercontinent breakup. *Tectonophysics*, 746:312–324.

Dal Zilio, L., van Dinther, Y., Gerya, T. V., and Pranger, C. C. (2018b). Seismic behaviour of mountain belts controlled by plate convergence rate. *Earth and Planetary Science Letters*, 482:81–92.

Davies, G. F. (1977). Viscous mantle flow under moving lithospheric plates and under subduction zones. *Geophysical Journal International*, 49(3):557–563.

Davies, J. H. and von Blanckenburg, F. (1995). Slab breakoff: a model of lithosphere detachment and its test in the magmatism and deformation of collisional orogens. *Earth and Planetary Science Letters*, 129(1-4):85–102.

Dewey, J., Helman, M., Knott, S., Turco, E., and Hutton, D. (1989). Kinematics of the western mediterranean. *Geological Society, London, Special Publications*, 45(1):265–283.

Duretz, T., Gerya, T. V., and May, D. A. (2011). Numerical modelling of spontaneous slab breakoff and subsequent topographic response. *Tectonophysics*, 502(1-2):244–256.

Erdős, Z., Huismans, R. S., and Beek, P. v. d. (2019). Control of increased sedimentation on orogenic fold-and-thrust belt structure–insights into the evolution of the western alps. *Solid Earth*, 10(2):391–404.

Faccenda, M. and Dal Zilio, L. (2017). The role of solid–solid phase transitions in mantle convection. *Lithos*, 268:198–224.

Faccenda, M., Minelli, G., and Gerya, T. (2009). Coupled and decoupled regimes of continental collision: Numerical modeling. *Earth and Planetary Science Letters*, 278(3-4):337–349.

Faccenna, C., Piromallo, C., Crespo-Blanc, A., Jolivet, L., and Rossetti, F. (2004). Lateral slab deformation and the origin of the western Mediterranean arcs. *Tectonics*, 23(1):TC1012.

Forsyth, D. and Uyeda, S. (1975). On the relative importance of the driving forces of plate motion. *Geophysical Journal International*, 43(1):163–200.

Froitzheim, N., Conti, P. t., and Van Daalen, M. (1997). Late cretaceous, synorogenic, low-angle normal faulting along the schlinig fault (switzerland, italy, austria) and its significance for the tectonics of the eastern alps. *Tectonophysics*, 280(3-4):267–293.

Fry, B., Deschamps, F., Kissling, E., Stehly, L., and Giardini, D. (2010). Layered azimuthal anisotropy of rayleigh wave phase velocities in the european alpine lithosphere inferred from ambient noise. *Earth and Planetary Science Letters*, 297(1-2):95–102.

Gerya, T. and Yuen, D. (2007). Robust characteristics method for modelling multiphase visco-elasto-plastic thermo-mechanical problems. *Physics of the Earth and Planetary Interiors*, 163(1):83–105.

Gerya, T. V. and Yuen, D. A. (2003). Characteristics-based marker-in-cell method with conservative finite-differences schemes for modeling geological flows with strongly variable transport properties. *Physics of the Earth and Planetary Interiors*, 140(4):293 – 318.

Handy, M. R., Schmid, S. M., Bousquet, R., Kissling, E., and Bernoulli, D. (2010). Reconciling plate-tectonic reconstructions of alpine tethys with the geological–geophysical record of spreading and subduction in the alps. *Earth-Science Reviews*, 102(3-4):121–158.

Jolivet, L., Faccenna, C., Huet, B., Labrousse, L., Le Pourhiet, L., Lacombe, O., Lecomte, E., Burov, E., Denele, Y., Brun, J.-P., et al. (2013). Aegean tectonics: Strain localisation, slab tearing and trench retreat. *Tectonophysics*, 597:1–33.

Kästle, E. D., Rosenberg, C., Boschi, L., Bellahsen, N., Meier, T., and El-Sharkawy, A. (2019). Slab break-offs in the alpine subduction zone. *Solid Earth Discussions*, 2019:1–16.

Király, Á., Capitanio, F. A., Funiciello, F., and Faccenna, C. (2016). Subduction zone interaction: Controls on arcuate belts. *Geology*, 44(9):715–718.

Kissling, E. (1993). Deep structure of the alps—what do we really know? *Physics of the Earth and Planetary Interiors*, 79(1-2):87–112.

Kissling, E. and Schlunegger, F. (2018). Rollback orogeny model for the evolution of the swiss alps. *Tectonics*, 37(4):1097–1115.

Lippitsch, R., Kissling, E., and Ansorge, J. (2003). Upper mantle structure beneath the alpine orogen from high-resolution teleseismic tomography. *Journal of Geophysical Research: Solid Earth*, 108(B8).

Lyon-Caen, H. and Molnar, P. (1989). Constraints on the deep structure and dynamic processes beneath the alps and adjacent regions from an analysis of gravity anomalies. *Geophysical Journal International*, 99(1):19–32.

Magni, V., Allen, M. B., van Hunen, J., and Bouilhol, P. (2017). Continental underplating after slab break-off. *Earth and Planetary Science Letters*, 474:59–67.

Magni, V., Faccenna, C., van Hunen, J., and Funiciello, F. (2013). Delamination vs. break-off: the fate of continental collision. *Geophysical Research Letters*, 40(2):285–289.

Magni, V., Faccenna, C., van Hunen, J., and Funiciello, F. (2014). How collision triggers backarc extension: Insight into mediterranean style of extension from 3-d numerical models. *Geology*, 42(6):511–514.

Malinverno, A. and Ryan, W. B. (1986). Extension in the tyrrhenian sea and shortening in the apennines as result of arc migration driven by sinking of the lithosphere.

Tectonics, 5(2):227–245.

McKenzie, D. P. (1969). Speculations on the consequences and causes of plate motions. *Geophysical Journal International*, 18(1):1–32.

Menant, A., Sternai, P., Jolivet, L., Guillou-Frottier, L., and Gerya, T. (2016). 3d numerical modeling of mantle flow, crustal dynamics and magma genesis associated with slab roll-back and tearing: The eastern mediterranean case. *Earth and Planetary Science Letters*, 442:93–107.

Platt, J., Behrmann, J., Cunningham, P., Dewey, J., Helman, M., Parish, M., Shepley, M., Wallis, S., and Western, P. (1989). Kinematics of the alpine arc and the motion history of adria. *Nature*, 337(6203):158.

Pusok, A. E., Kaus, B. J., and Popov, A. A. (2018). The effect of rheological approximations in 3-d numerical simulations of subduction and collision. *Tectonophysics*, 746:296–311.

Royden, L. H. (1993). The tectonic expression slab pull at continental convergent boundaries. *Tectonics*, 12(2):303–325.

Schlunegger, F. and Kissling, E. (2015). Slab rollback orogeny in the alps and evolution of the swiss molasse basin. *Nature communications*, 6.

Schmid, S. M., Pfiffner, O., Froitzheim, N., Schönborn, G., and Kissling, E. (1996). Geophysical-geological transect and tectonic evolution of the swiss-italian alps. *Tectonics*, 15(5):1036–1064.

Singer, J., Diehl, T., Husen, S., Kissling, E., and Duretz, T. (2014). Alpine lithosphere slab rollback causing lower crustal seismicity in northern foreland. *Earth and Planetary Science Letters*, 397:42–56.

Spada, M., Bianchi, I., Kissling, E., Agostinetti, N. P., and Wiemer, S. (2013). Combining controlled-source seismology and receiver function information to derive 3-D moho topography for italy. *Geophysical Journal International*, 194(2):1050–1068.

Stevenson, D. and Turner, J. (1977). Angle of subduction. *Nature*, 270(5635):334–336.

Turcotte, D. and Oxburgh, E. (1967). Finite amplitude convective cells and continental drift. *Journal of Fluid Mechanics*, 28(01):29–42.

Uyeda, S. and Kanamori, H. (1979). Back-arc opening and the mode of subduction. *Journal of Geophysical Research: Solid Earth*, 84(B3):1049–1061.

van Dinther, Y., Gerya, T., Dalguer, L., Mai, P. M., Morra, G., and Giardini, D. (2013). The seismic cycle at subduction thrusts: Insights from seismo-thermo-mechanical models. *Journal of Geophysical Research: Solid Earth*, 118(12):6183–6202.

van Hunen, J. and Allen, M. B. (2011). Continental collision and slab break-off: a comparison of 3-d numerical models with observations. *Earth and Planetary Science Letters*, 302(1-2):27–37.

Whipple, K. X. (2009). The influence of climate on the tectonic evolution of mountain belts. *Nature geoscience*, 2(2):97.

Whipple, K. X. and Meade, B. J. (2006). Orogen response to changes in climatic and tectonic forcing. *Earth and Planetary Science Letters*, 243(1-2):218–228.

Willett, S. D. (1999). Orogeny and orography: The effects of erosion on the structure of mountain belts. *Journal of Geophysical Research: Solid Earth*,

104(B12):28957–28981.

Willett, S. D. (2010). Late neogene erosion of the alps: A climate driver? *Annual Review of Earth and Planetary Sciences*, 38:411–437.

Supporting Information References

[496] Allmann, B. P., & Shearer, P. M. (2009). Global variations of stress drop for moderate to large earthquakes. *Journal of Geophysical Research: Solid Earth*, *114*(B1).

Ampuero, J.-P., & Ben-Zion, Y. (2008). Cracks, pulses and macroscopic asymmetry of dynamic rupture on a bimaterial interface with velocity-weakening friction. *Geophysical Journal International*, *173*(2), 674–692.

Crameri, F., Schmeling, H., Golabek, G., Duretz, T., Orendt, R., Buiter, S., ... Tackley, P. (2012). A comparison of numerical surface topography calculations in geodynamic modelling: An evaluation of the 'sticky air'method. *Geophysical Journal International*, *189*(1), 38–54.

Dal Zilio, L., van Dinther, Y., Gerya, T. V., & Pranger, C. C. (2018, 1). Seismic behaviour of mountain belts controlled by plate convergence rate. *Earth and Planetary Science Letters*, *482*, 81–92.

Del Gaudio, P., Di Toro, G., Han, R., Hirose, T., Nielsen, S., Shimamoto, T., & Cavallo, A. (2009). Frictional melting of peridotite and seismic slip. *Journal of Geophysical Research: Solid Earth*, *114*(B6).

Den Hartog, S., Niemeijer, A., & Spiers, C. (2012). New constraints on megathrust slip stability under subduction zone p–t conditions. *Earth and Planetary Science Letters*, *353*, 240–252.

Di Toro, G., Han, R., Hirose, T., De Paola, N., Nielsen, S., Mizoguchi, K., ... Shimamoto, T. (2011). Fault lubrication during earthquakes. *Nature*, *471*(7339), 494–498.

Doin, M.-P., & Henry, P. (2001). Subduction initiation and continental crust recycling: the roles of rheology and eclogitization. *Tectonophysics*, *342*(1-2), 163–191.

Duretz, T., Gerya, T. V., & May, D. A. (2011). Numerical modelling of spontaneous slab breakoff and subsequent topographic response. *Tectonophysics*, *502*(1-2), 244–256.

Evans, B., & Goetze, C. (1979). The temperature variation of hardness of olivine and its implication for polycrystalline yield stress. *Journal of Geophysical Research: Solid Earth*, *84*(B10), 5505–5524.

Faccenda, M., & Dal Zilio, L. (2017). The role of solid–solid phase transitions in mantle convection. *Lithos*, *268*, 198–224.

Gerya, T. (2010). *Introduction to numerical geodynamic modelling*. Cambridge University Press.

Gerya, T., & Yuen, D. (2007). Robust characteristics method for modelling multiphase visco-elasto-plastic thermo-mechanical problems. *Physics of the Earth and Planetary Interiors*, *163*(1), 83–105.

Ito, K., & Kennedy, G. C. (1971). An experimental study of the basalt-garnet granulite-eclogite transition. *The structure and physical properties of the Earth's crust*, *14*, 303–314.

Kameyama, M., Yuen, D. A., & Karato, S.-I. (1999). Thermal-mechanical effects of low-temperature plasticity (the peierls mechanism) on the deformation of a viscoelastic shear zone. *Earth and Planetary Science Letters*, *168*(1-2), 159–172.

Karato, S.-i., Riedel, M. R., & Yuen, D. A. (2001). Rheological structure and deformation of subducted slabs in the mantle transition zone: implications for mantle circulation and deep earthquakes. *Physics of the Earth and Planetary Interiors*, *127*(1-4), 83–108.

Katayama, I., & Karato, S.-i. (2008). Low-temperature, high-stress deformation of olivine under water-saturated conditions. *Physics of the Earth and Planetary Interiors*, *168*(3), 125–133.

Krystopowicz, N. J., & Currie, C. A. (2013). Crustal eclogitization and lithosphere delamination in orogens. *Earth and Planetary Science Letters*, *361*, 195–207.

Li, Z.-H., Liu, M., & Gerya, T. (2016). Lithosphere delamination in continental collisional orogens: A systematic numerical study. *Journal of Geophysical Research: Solid Earth*, *121*(7), 5186–5211.

Lu, G., Kaus, B. J., & Zhao, L. (2011). Thermal localization as a potential mechanism to rift cratons. *Physics of the Earth and Planetary Interiors*, *186*(3-4), 125–137.

Nikolaeva, K., Gerya, T., & Marques, F. (2010). Subduction initiation at passive margins: Numerical modeling. *Journal of Geophysical Research: Solid Earth (1978–2012)*, *115*(B3).

Prager, W., & Drucker, D. (1952). Soil mechanics and plastic analysis or limit design, 0. *Appi. Math*,

10(2), 157–165.

Ranalli, G. (1995). *Rheology of the earth*. Springer.

Rudnick, R. L., & Fountain, D. M. (1995). Nature and composition of the continental crust: a lower crustal perspective. *Reviews of geophysics*, *33*(3), 267–309.

Schultz, R. (1995). Limits on strength and deformation properties of jointed basaltic rock masses. *Rock Mechanics and Rock Engineering*, *28*(1), 1–15.

Seno, T. (2009). Determination of the pore fluid pressure ratio at seismogenic megathrusts in subduction zones: Implications for strength of asperities and andean-type mountain building. *Journal of Geophysical Research: Solid Earth*, *114*(B5).

Sibson, R. H. (1994). Crustal stress, faulting and fluid flow. *Geological Society, London, Special Publications*, *78*(1), 69–84. Retrieved from `http://sp.lyellcollection.org/content/78/1/69` doi: 10.1144/GSL.SP.1994.078.01.07

Turcotte, D., & Schubert, G. (2002). *Geodynamics*. Cambridge University Press.

van Dinther, Y., Gerya, T., Dalguer, L., Mai, P. M., Morra, G., & Giardini, D. (2013). The seismic cycle at subduction thrusts: Insights from seismo-thermo-mechanical models. *Journal of Geophysical Research: Solid Earth*, *118*(12), 6183–6202.

Van Heck, H., & Tackley, P. (2008). Planforms of self-consistently generated plates in 3d spherical geometry. *Geophysical Research Letters*, *35*(19).

Wells, D. L., & Coppersmith, K. J. (1994). New empirical relationships among magnitude, rupture length, rupture width, rupture area, and surface displacement. *Bulletin of the seismological Society of America*, *84*(4), 974–1002.

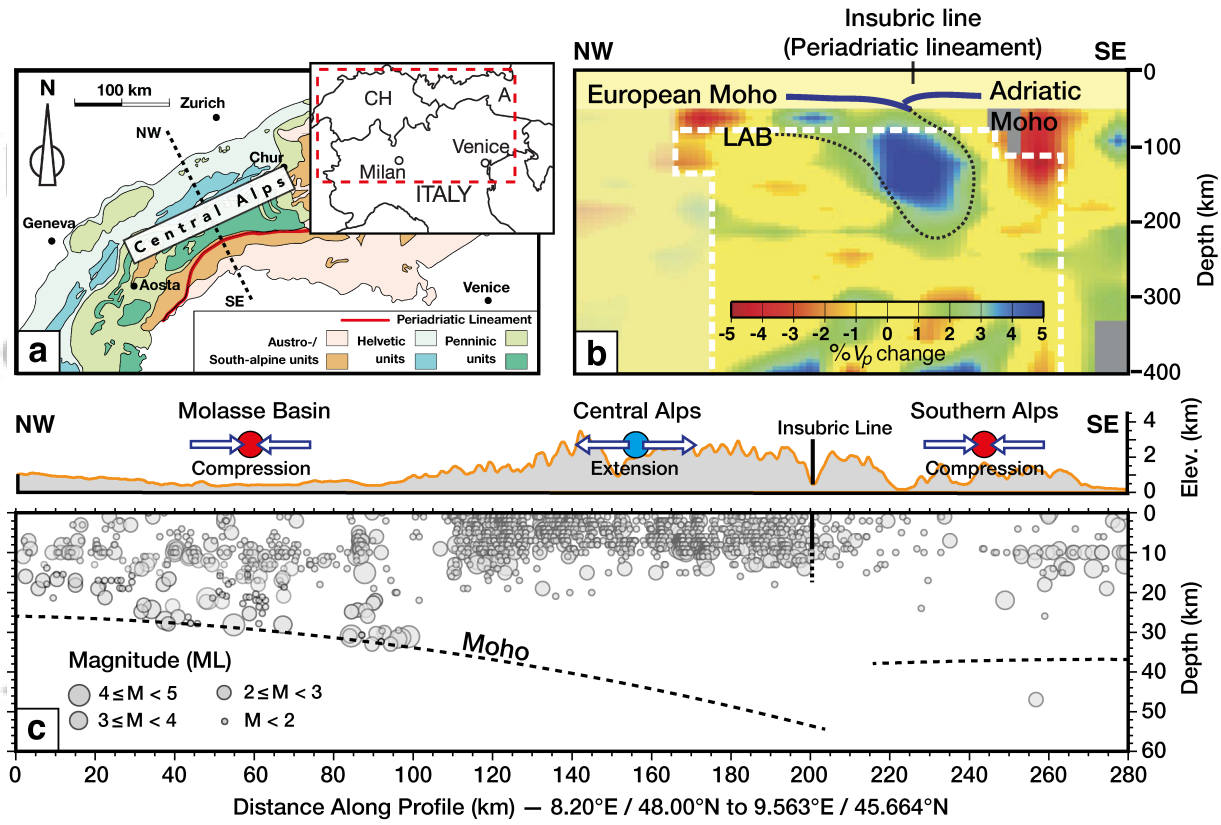

Figure 1. **a**, Inset map illustrating the Alps and its foreland basin along with the section discussed in this study. **b**, Teleseismic tomography cross-section illustrating the geometry of the European slab beneath the central Alps (Lippitsch et al., 2003). White dashed line indicate the region with high-resolution. The figure shows lateral variations of P-wave velocity Vp beneath the Moho. **c**, Topographic profile and vertical cross-section approximately perpendicular to the strike of the Central Alps. Transparent gray circles represent earthquake hypocenters (Singer et al., 2014). Dashed black lines indicate the Moho with a ±3 km uncertainty of the depth (Spada et al., 2013).

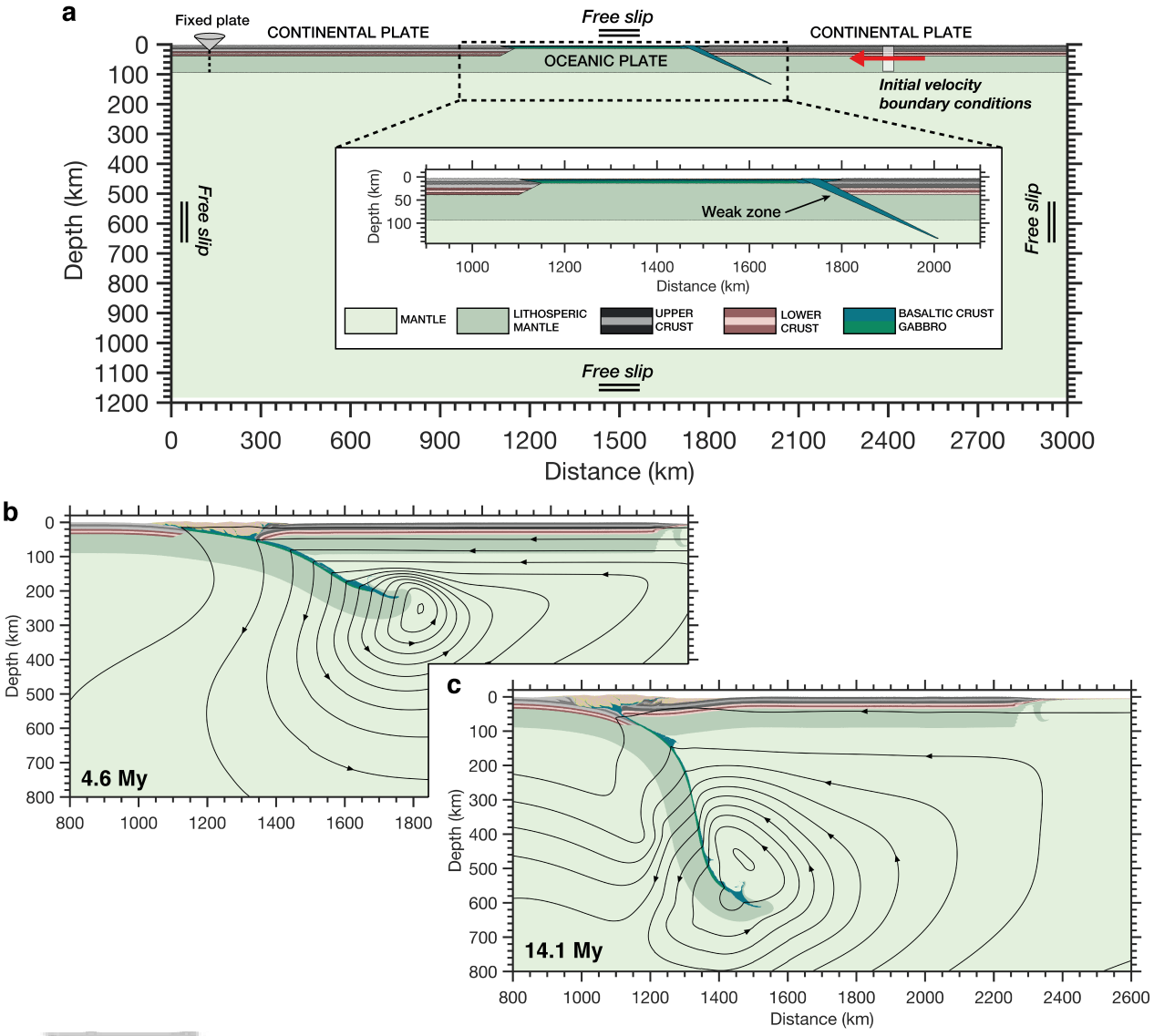

Figure 2. **a**, 2-D initial setup. Initial composition map including boundary conditions. The model simulates subduction initiation through the use of a fixed convergence rate (red arrow) on the upper plate until ∼200 km of oceanic crust has been subducted. Zoom shows the oceanic plate and pre-imposed weak zone to initiate subduction. **b**–**c**, Dynamic evolution of a spontaneously retreating subducting plate and mantle-lithosphere interaction after 4.6 and 14.1 My. The superimposed stream function contours display the effect of subduction-induced trench suction and return flow in mantle, which maintain the upper plate coupled with the retreating slab.

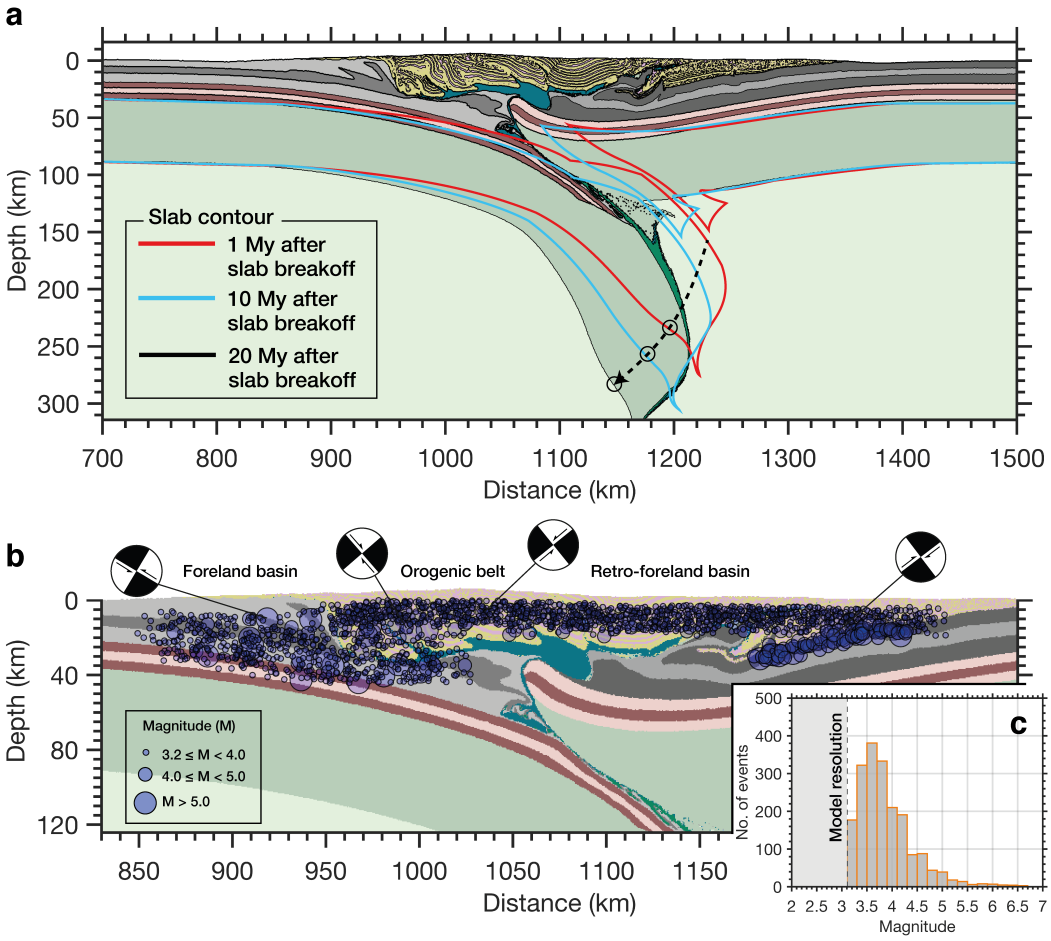

Figure 3. **a**, Post-collisional evolution with superimposed contours of the slab geometries at 1 and 10 My after slab breakoff. Compositional map shows the final structure 20 My after slab breakoff. Evolution of the orogen is driven by slow slab rollback and delamination of crustal material. **b**, Short-term seismicity pattern of the reference model. Cluster of seismicity and the inferred 2-D focal mechanisms display a broad pattern of different style of faulting, which are consistent with the local tectonic regime. **c**, Histograms of all events and the corresponding magnitude.

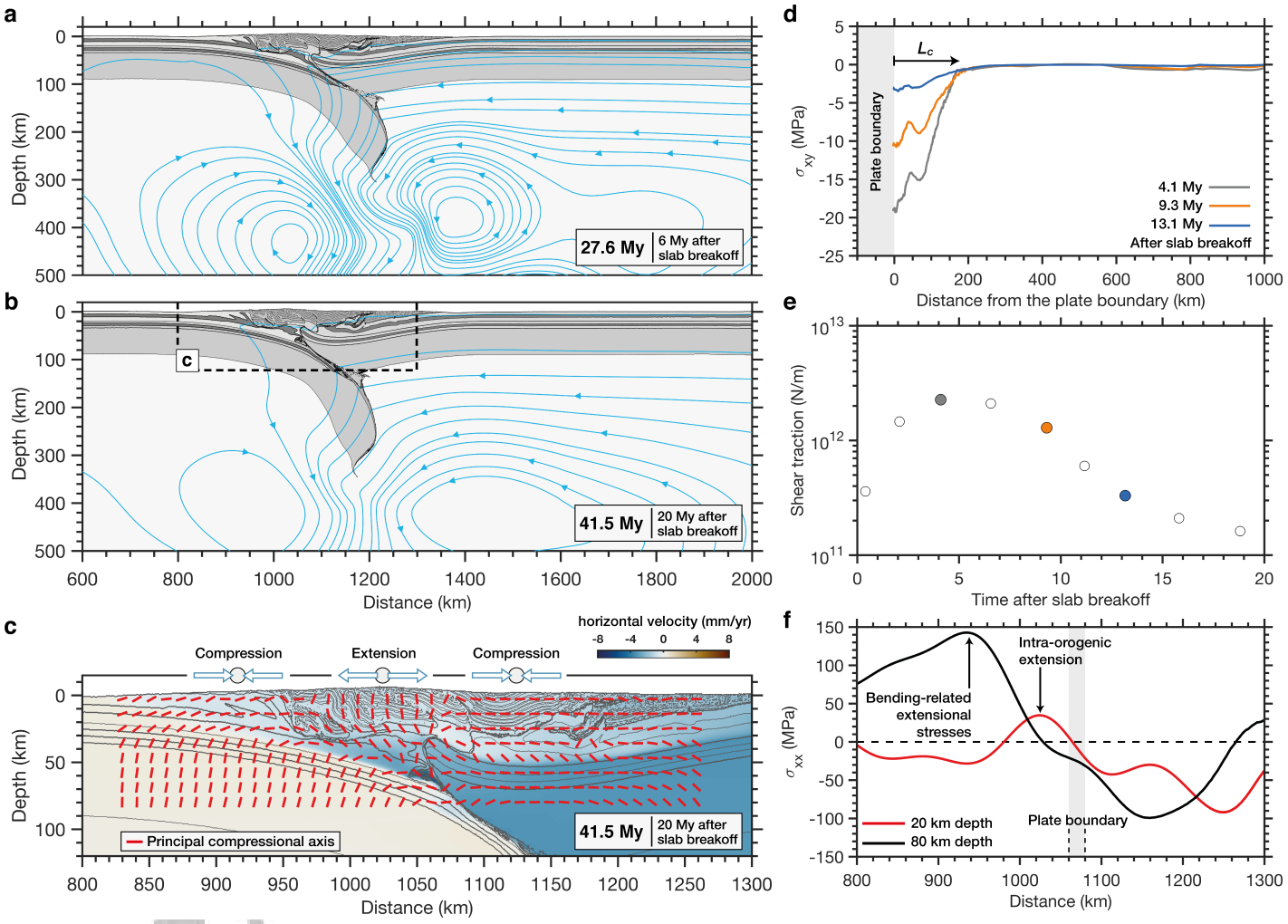

Figure 4. **a**–**b**, Key stages of mantle-lithosphere 27.6 and 41.5 My after slab breakoff. Rock composition (gray scale map) and contour of stream function in light-blue display sinking and retreat of the remaining slab, which cause poloidal mantle flow and basal shear stresses beneath the upper plate. **c**, Zoom of the spatial distribution of horizontal velocity. Red bars indicate orientation of maximum (compression) principal stresses. The inferred stress axes show a broad pattern of different tectonic regimes throughout the orogen (compression-extension-compression), which are consistent with the style of faulting and seismicity pattern. **d**, Profiles of basal shear stress for different post-collisional stages of the reference model. **e**, Time evolution of shear traction at the base of the upper plate. Gray, orange and blue markers correspond to the profile shown in panel **d**. **f**, Profiles of horizontal stress throughout the orogen at 20 and 80 km depth (time: 41.5 My – 20 My after slab breakoff). Positive is extension, negative is compression.